**DOI**: 10.21608/sjsci.2025.408735.1300

# Study of infinite nuclear matter and finite nuclei properties using the phenomenological forces based on Brueckner-Hartree-Fock calculations

Khaled S.A. Hassaneen\*,1, Rehab Ragab1, and Hoda M. Abou-Elsebaa1,2

Received: 29st July 2025, Revised: 13st September 2025, Accepted: 1st October 2025.

Published online: 12st November 2025.

#### Abstract:

We present a comprehensive investigation of nuclear matter saturation properties and finite nuclei characteristics, emphasizing the critical role of three-body forces (3BF) in bridging microscopic interactions with macroscopic nuclear phenomena. Using Brueckner-Hartree-Fock (BHF) theory with modern nucleon-nucleon potentials (AV14, AV18, CD-Bonn, N3LO), we demonstrate that two-body forces alone fail to reproduce empirical saturation properties ( $\rho_0 = 0.17 \text{ fm}^{-3}$ , E/A = -15.78 MeV). The inclusion of consistent 3BF yields remarkable agreement, particularly for the chiral N3LO potential. Our extension to finite nuclei employs energy density functional methods with optimized Skyrme parameterizations (SKM\*), providing binding energies and charge radii in excellent agreement with experimental data. The study highlights the tensor force's influence on the equation of state and introduces improved density functionals that address previous limitations in describing neutron-rich systems. These results establish a robust connection between ab initio nuclear matter calculations and finite-nuclei phenomenology, with significant implications for nuclear structure.

**keywords:** nuclear matter, finite nuclei, 3-nucleon forces, realistic NN interaction.

#### 1 Introduction

The microscopic description of nuclear matter and finite nuclei is a central problem in nuclear physics and astrophysics. Efforts to link ab initio many-body calculations with phenomenological energy density functionals (EDFs) have gained momentum in recent decades [1,2]. The Brueckner-Hartree-Fock (BHF) method provides a framework to describe infinite nuclear matter starting from realistic nucleon-nucleon (NN) interactions [3,4]. Three-body forces (3BF), such as Urbana IX [5], are critical for reproducing empirical saturation properties and the stiffness of the EOS at high densities [6,7]. Also it is crucial for accurately describing the behavior of nuclei, especially those with more than three nucleons. Rafi et al. [8] presented a microscopic study of symmetric nuclear matter and the nucleon-nucleus optical potential within the BHF framework, employing various two-nucleon interactions and incorporating 3BF using the Urbana IX and phenomenological density-dependent models. The study demonstrated that two-body forces alone fail to reproduce empirical saturation properties of nuclear matter, while the inclusion of 3BF significantly improves agreement with observed saturation density and binding energy per nucleon.

The BHF approach is a microscopic many-body framework that provides a self-consistent description of in-medium nucleon-nucleon interactions [9,10]. It relies on the calculation of the in-medium reaction matrix G, which satisfies the Bethe-Goldstone integral equation. Despite its success, the two-body force (2BF) calculations within BHF alone often fail to reproduce certain nuclear matter properties, particularly the empirical saturation point characterized by a saturation density  $\rho_0=0.17\,\mathrm{fm}^{-3}$  and binding energy per nucleon  $E/A\approx-16\,\mathrm{MeV}$  [11,12]. To address this, the inclusion of 3BF has become essential. These 3BF corrections account for additional correlations in the system and are known to significantly stiffen the EOS at high densities.

The effective nucleon-nucleon interactions used in this work include several modern potentials: Argonne V18 (AV18) [13], Argonne V14 (AV14) [14],

<sup>&</sup>lt;sup>1</sup> Physics Department, Faculty of Science, Sohag University, 82425-Sohag, Egypt.

<sup>&</sup>lt;sup>2</sup> Physics Department, College of Science, Taibah University, Medina, Saudi Arabia.

<sup>\*</sup>Corresponding Author: khaled.hassaneen@science.sohag.edu.eg.

CD-Bonn [15], and chiral N3LO [16] pseudopotentials. Each potential introduces unique features that influence the predicted EOS [17]:

- -Argonne V18 is a high-precision, local potential with 18 operator components including strong tensor terms and charge-dependence corrections [13]. Its pronounced tensor force makes it ideal for describing spin-dependent phenomena but also leads to a stiffer EOS at supra-saturation densities [18].
- **-Argonne V14**, an earlier version, includes 14 operator terms and lacks certain refinements of AV18, yielding a comparatively softer EOS [19].
- **–CD-Bonn** is a nonlocal, relativistic one-boson exchange potential defined in momentum space [15]. Its nonlocality reduces the strength of the tensor force relative to AV18, producing a softer EOS that is well-suited for relativistic many-body calculations [20].
- -Chiral N3LO arises from chiral effective field theory (EFT), which systematically expands NN interactions in powers of momenta consistent with quantum chromodynamics (QCD) symmetries [16]. N3LO includes long-range pion-exchange terms and short-range contact interactions, regularized at high momenta, leading to a softer EOS and excellent applicability to neutron-rich systems and astrophysical studies [21].

The interplay between these NN potentials and the Skyrme energy density functional is examined in this work to constrain nuclear matter properties, including the symmetry energy and its density dependence and incompressibility. The EOS predictions are benchmarked against ab initio calculations, empirical data, and constraints from heavy-ion collision experiments and neutron star observations [22, 23].

The methodology developed by Cao et al. [24] and very recently Vidana et al. [25] established an essential framework for linking microscopic BHF calculations to Skyrme-type energy density functionals (EDFs). The BHF results for symmetric nuclear matter with the inclusion of 3BF, they are parametrized an effective Skyrme interaction successfully for reproducing the empirical saturation density and binding energy per nucleon. Their LNS Skyrme functional provided a computationally efficient tool for finite nuclei calculations while retaining the predictive power of microscopic many-body theory. However, certain limitations persisted, such as a tendency to underestimate nuclear charge radii and challenges in describing neutron-rich systems beyond moderate asymmetry. Our present work builds directly upon this foundation, extending it by incorporating a wider and more modern set of NN potentials, including AV18, AV14, CD-Bonn, and the chiral N3LO interaction.

#### 2 Theoretical Model

#### 2.1 BHF Without Three-Body Forces

The BHF method is based on the Bethe-Goldstone equation for the in-medium G-matrix [3,26]:

$$G(\boldsymbol{\omega}) = v_{NN} + v_{NN} \sum_{k_1, k_2} \frac{|k_1 k_2\rangle Q(k_1, k_2) \langle k_1 k_2|}{\boldsymbol{\omega} - \boldsymbol{\varepsilon}(k_1) - \boldsymbol{\varepsilon}(k_2)} G(\boldsymbol{\omega}), \quad (1)$$

where  $v_{NN}$  is the bare nucleon-nucleon interaction, Q is the Pauli operator projecting onto unoccupied states, and  $\varepsilon(k)$  is the single-particle energy given by:

$$\varepsilon(k) = \frac{\hbar^2 k^2}{2m} + U(k),\tag{2}$$

with U(k) as the single-particle potential computed self-consistently:

$$U(k) = \sum_{k' \le k_E} \langle kk' | G(\omega) | kk' \rangle_A. \tag{3}$$

#### 2.2 BHF with Three-Body Forces

To account for 3BF effects, the Hamiltonian includes an additional term:

$$H = \sum_{i} -\frac{\hbar^2}{2m} \nabla_i^2 + \sum_{i < j} v_{ij} + \sum_{i < j < k} V_{ijk}, \tag{4}$$

where  $V_{ijk}$  represents the three-nucleon interaction, implemented through the Urbana model modified by Baldo [27] as:

$$V_{3BF} = \sum_{i < j < k} \left( V_{ijk}^{2\pi} + V_{ijk}^R \right), \tag{5}$$

with  $V_{ijk}^{2\pi}$  representing two-pion exchange contributions and  $V_{ijk}^R$  modeling short-range repulsion. The 3BF is reduced to an effective density-dependent two-body force for use in the BHF framework. The EOS for nuclear matter with 3BF is calculated self-consistently:

$$\frac{E}{A}(\rho) = \frac{3\hbar^2}{10m} (3\pi^2 \rho/2)^{2/3} + \frac{1}{2\rho} \sum_{k,k' \le k_F} \left[ \langle kk' | G_{2BF} | kk' \rangle_A \right] + \frac{1}{4\rho} \sum_{k'' < k_F} \left[ \langle kk'k'' | V_{3BF} | kk'k'' \rangle_A \right].$$
(6)

# **Research Article**

# 2.3 Skyrme Energy Density Functional

The Skyrme energy density functional is expressed as [1]:

$$H = \frac{\hbar^{2}}{2m}\tau + \frac{t_{0}}{2}\left[(1+x_{0})\rho^{2} - (x_{0} + \frac{1}{2})\sum_{q}\rho_{q}^{2}\right]$$

$$+ \frac{t_{3}}{12}\rho^{\alpha}\left[(1+x_{3})\rho^{2} - (x_{3} + \frac{1}{2})\sum_{q}\rho_{q}^{2}\right]$$

$$+ \frac{1}{4}\left[t_{1}(1+x_{1}) + t_{2}(1+x_{2})\right]\rho\tau$$

$$- \frac{1}{4}\left[t_{1}(x_{1} + \frac{1}{2}) - t_{2}(x_{2} + \frac{1}{2})\right]\sum_{q}\rho_{q}\tau_{q}$$

$$+ \frac{1}{16}\left[3t_{1}(1+x_{1}) - t_{2}(1+x_{2})\right](\nabla\rho)^{2}$$

$$- \frac{1}{16}\left[3t_{1}(x_{1} + \frac{1}{2}) + t_{2}(x_{2} + \frac{1}{2})\right]\sum_{q}(\nabla\rho_{q})^{2}$$

$$+ \frac{W_{0}}{2}\sum_{q}\mathbf{J}_{q}\cdot\nabla\rho_{q},$$
(7)

where  $\rho_q$  and  $\tau_q$  are the density and kinetic density for nucleon type q, and  $\mathbf{J}_q$  is the spin-current density.

# 2.4 Skyrme Energy and Parameter Fitting (SKM\*)

The Skyrme energy per nucleon reads [28]:

$$\frac{E}{A}(\rho)_{SKM*} = \frac{3}{5} \frac{\hbar^2}{2m} \left(\frac{3\pi^2}{2}\rho\right)^{2/3} 
+ \frac{3}{8} t_0 \rho + \frac{1}{16} t_3 \rho^{\alpha+1} 
+ \frac{1}{16} \left[3t_1 + t_2(5 + 4x_2)\right] \left(\frac{3\pi^2}{2}\right)^{2/3} \rho^{5/3}.$$
(8)

At saturation density  $\rho_0$ , the conditions for pressure and incompressibility are imposed:

$$\frac{d(E/A)}{d\rho}\Big|_{\rho_0} = 0, \quad K_0 = 9\rho_0^2 \frac{d^2(E/A)}{d\rho^2}\Big|_{\rho_0}.$$
 (9)

The symmetry energy is:

$$J = \frac{1}{3} \frac{\hbar^2}{2m} \left( \frac{3\pi^2}{2} \rho_0 \right)^{2/3} + \frac{1}{8} t_0 (2x_0 + 1) \rho_0 + \frac{1}{48} t_3 (2x_3 + 1) \rho_0^{\alpha + 1}.$$
 (10)

The parameters  $t_0, t_1, t_2, t_3, x_0, x_1, x_2, x_3$  are determined by minimizing

$$\chi^{2} = \sum_{i} \left[ \frac{E/A(\rho_{i})_{BHF} - E/A(\rho_{i})_{Skyrme}}{\Delta E/A} \right]^{2}, \quad (11)$$

# SOHAG JOURNAL OF SCIENCES

subject to effective mass constraints:

$$\frac{m^*}{m} = 1 + \frac{m}{\hbar^2} \frac{\rho_0}{4} \left[ t_1(1+x_1) + t_2(1+x_2) \right]. \tag{12}$$

Solving gives:

$$t_1(1+x_1)+t_2(1+x_2) = \frac{4\hbar^2}{m} \frac{1}{\rho_0} \left(\frac{m}{m^*}-1\right).$$
 (13)

This extended fitting procedure determines all Skyrme parameters  $(t_0,t_1,t_2,t_3,x_0,x_1,x_2,x_3)$  directly from the BHF EOS including three-body forces. By solving these equations, the SKM\* [28] parameters are fitted as:

$$t_0 = -2645 \,\text{MeV fm}^3, t_1 = 410 \,\text{MeV fm}^5,$$
 (14)

$$t_2 = -135 \,\text{MeV fm}^5, t_3 = 15595 \,\text{MeV fm}^{3(1+\alpha)},$$
 (15)

$$x_0 = 0.09, x_1 = 0.0, x_2 = 0.0, x_3 = 0.0, \alpha = 1/6.$$
 (16)

#### 3 Finite Nuclei Calculations

## 3.1 Two-Parameter Fermi Density Profiles

For finite nuclei, proton and neutron densities are modeled using the two-parameter Fermi (2pF) function:

$$\rho_q(r) = \frac{\rho_{0,q}}{1 + \exp\left(\frac{r - R_q}{a_q}\right)},\tag{17}$$

where  $\rho_{0,q}$  is the central density,  $R_q$  is the half-density radius, and  $a_q$  is the diffuseness parameter. These parameters are determined by fitting to the EOS derived from BHF+3BF.

#### 3.2 Total Energy of Finite Nuclei

The optimized functional is applied to finite nuclei using 2pF density distributions for protons and neutrons [29]. The total energy includes bulk, surface, spin-orbit, Coulomb, and pairing contributions:

$$E_{\text{nucleus}} = \int d^3 r \left[ H_{\text{SKM*}}(\rho, \tau, \mathbf{J}) + H_{\text{Coul}} \right] + E_{\text{pair}} + E_{\text{CM}}.$$
(18)

This approach enables a direct connection between microscopic nuclear interactions and phenomenological Skyrme functionals constrained by both terrestrial and astrophysical data.

## 3.3 Coulomb Component

The Coulomb energy includes direct and exchange terms [30]:

$$H_{\text{Coul}} = \frac{e^2}{2} \int d^3 r \int d^3 r' \frac{\rho_p(r)\rho_p(r')}{|r - r'|} - \frac{3e^2}{4} \left(\frac{3}{\pi}\right)^{1/3} \rho_p^{4/3}(r).$$
(19)

#### 3.4 Spin-Orbit Contribution

The spin-orbit term in the energy density functional is expressed as:

$$H_{SO} = \frac{W_0}{2} \sum_{q} \mathbf{J}_q \cdot \nabla \rho_q, \tag{20}$$

where  $W_0$  is the spin-orbit coupling strength.

#### 4 Results and Discussion

#### 4.1 Nuclear matter properties

The Figure 1 presents two plots of the nuclear Equation of State (EOS), specifically the energy per nucleon (E/A) as a function of the baryon density  $(\rho, infm^{-3})$ . This graph provides insights into how different nuclear force models predict the behavior of symmetric nuclear matter under interaction. The left panel shows results from BHF calculations without including three-body forces, while the right panel includes the effects of 3BF. The curves represent different nucleon-nucleon interaction potentials: AV14, AV18, CD-Bonn, and N3LO, each corresponding to a different line and symbol type. On both panels, a green cross-hatched square marks the empirical saturation nuclear matter  $(\rho_0 = 0.17 fm^{-3}, E/A_0 = -16 MeV)$ , where nuclear matter is most stable. In the left panel BHF, none of the models perfectly reproduce the empirical saturation point, with most underbinding (predicting less negative energy per nucleon) or saturating at the wrong density, indicating the insufficiency of two-body interactions alone. However, in the right panel, the inclusion of three-body forces improves the agreement significantly, as all four interactions now predict saturation properties that lie much closer to the empirical data point. This demonstrates the crucial role of three-body forces in realistic nuclear matter calculations, as they provide additional repulsion at higher densities, which stiffens the EOS and aligns theoretical predictions with experimental observations. The general trend in both panels shows that energy per nucleon decreases with increasing density until it reaches a minimum (saturation), after which it rises steeply due to increasing repulsive interactions, illustrating the balance between nuclear attraction at low densities and repulsion at high densities that governs the stability of nuclear matter.

As shown in Tables 1 and 2, we confirm the essential role of 3BF corrections in reproducing empirical saturation properties. Without 3BFs, all potentials exhibit significant deviations from the empirical saturation point, predicting either too high or too low incompressibility  $K_0$ . Including 3BFs shifts the predicted values of  $\rho_0$ , E/A, and  $K_0$  closer to experiment. For instance, AV18 with 3BF yields  $\rho_0 = 0.17 \, \mathrm{fm}^{-3}$  and  $K_0 = 262 \, \mathrm{MeV}$ , in excellent agreement with empirical data. The diversity of

NN interactions employed in our work provides insights into the sensitivity of Skyrme parameter fitting to the underlying microscopic inputs, with AV18 predicting a relatively stiff EOS and CD-Bonn and N3LO producing softer EOSs.

Figure 2 shows the saturation points of nuclear matter predicted by various nuclear interaction models, compared against the empirical saturation point, providing insight into the so-called Coester line [31] behavior. Each point represents the saturation E/A versus the corresponding saturation density  $\rho_0$  for a specific nucleon-nucleon potential model. The empirical values are marked by dashed lines at E/A = -16MeV and  $\rho_0 = 0.17 fm^{-3}$ , indicating the experimentally known most stable configuration of symmetric nuclear matter. Red squares denote the empirical point (EXP) and saturation predictions from different potentials that include three-body forces, while blue circles represent predictions from BHF calculations using only two-body forces. Additionally, the green diamond labeled "SKM\*" marks a point from a phenomenological Skyrme-type energy density functional, used as a benchmark. A clear trend emerges: models that consider only two-body forces (blue circles) predict saturation points that deviate significantly from the empirical values, either overbinding (more negative E/A) or predicting much higher densities—evident especially in the N3LO BHF and CD-Bonn BHF cases. These points fall along what is known as the Coester line, a correlation line where two-body interactions tend to cluster, showing an inverse relationship between binding energy and saturation density but missing the empirical point. In contrast, models including three-body forces (red squares) align much closer to the empirical saturation point, indicating that 3BFs are essential to reproduce realistic nuclear matter properties. This supports the conclusion that while two-body forces alone can model nucleon interactions qualitatively, they are insufficient to capture the correct saturation behavior quantitatively. Thus, the plot highlights the Coester line as a fundamental limitation of two-body-only calculations and emphasizes the crucial role of three-body interactions in accurately describing the nuclear equation of state.

The tensor component of the nucleon-nucleon interaction plays a critical role in determining the behavior of nuclear matter, particularly the EOS and saturation properties. Tensor forces, which arise mainly from pion exchange in NN interactions, induce strong correlations between nucleons and mix different angular momentum states, such as S and D waves in the deuteron. The strength of the tensor force is often quantified through the D-state probability  $(P_D)$ , which measures the admixture of D-wave components in the predominantly S-wave bound state.

Among the potentials studied, AV18 exhibits a relatively strong tensor component, reflected in a high  $(P_D \approx 5.76\%)$ . This strong tensor interaction leads to increased short-range correlations and a stiffer EOS, as

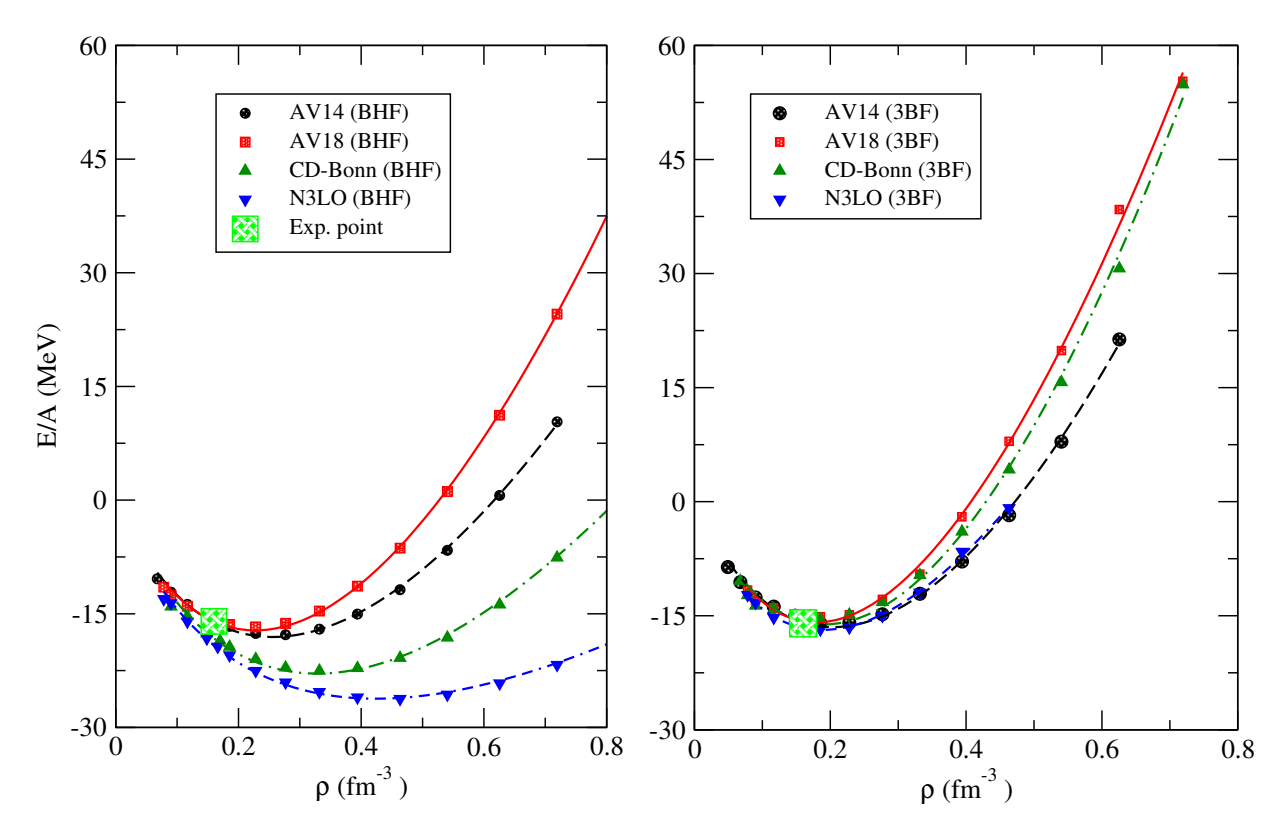


Figure 1: Equation of state (EOS) of symmetric nuclear matter: energy per nucleon E/A versus density  $\rho$  for various NN interactions in BHF. Left: two-body forces only. Right: including three-body forces (3BF). The shaded square shows empirical saturation. Each line represents the optimized SKM\* functional fitted to the EOS curve.

seen in Table 1. Consequently, AV18 predicts a more repulsive behavior at high densities and requires significant three-body force (3BF) contributions to reproduce empirical saturation properties. The saturation density with AV18+3BF ( $\rho_0 = 0.17 fm^{-3}$ ) shifts closer to experiment but remains slightly above the empirical value, indicating residual stiffness due to tensor correlations.

In contrast, CD-Bonn, a nonlocal potential, exhibits a weaker tensor component  $(P_D \approx 4.85\%)$ , resulting in reduced short-range correlations and a softer EOS. This manifests in a more attractive behavior at moderate densities, leading to saturation densities ( $\rho_0 = 0.18 fm^{-3}$ ) and incompressibility closer to empirical constraints even before including 3BF effects. Similarly, N3LO, derived from chiral effective field theory (EFT), is designed with a softer tensor component and yields  $(P_D \approx 4.51\%)$ , making it the most attractive among the potentials considered.

AV14, an earlier generation potential, also has a relatively strong tensor force  $(P_D \approx 5.66\%)$ , leading to behavior similar to AV18 but with subtle differences in the intermediate-range interactions. Like AV18, AV14 predicts a stiff EOS at high densities and relies on 3BFs to achieve a realistic saturation point.

These trends highlight the direct correlation between the tensor force strength (as reflected in  $(P_D)$  and the predicted EOS stiffness. Potentials with stronger tensor components tend to push saturation points toward higher densities and energies, emphasizing the necessity of incorporating 3BF corrections to counteract the repulsive effects of short-range correlations.

This observation is consistent with earlier studies by Baldo et al. [4], where potentials with reduced tensor strength, like CD-Bonn, were found to predict more realistic saturation properties without requiring excessively large 3BF contributions. Our results reaffirm these findings and demonstrate that the careful treatment of tensor forces and 3BFs is essential for constructing energy density functionals applicable to both symmetric and asymmetric nuclear matter.

**Table 1:** Nuclear matter saturation properties calculated with different interaction models. Shown are saturation density  $(\rho_0)$ , binding energy per nucleon  $(E/A_0)$ , incompressibility  $(K_0)$ , symmetry energy J and slope parameter L.

*	•				
Model	$\rho_0  ({\rm fm}^{-3})$	$E/A_0$ (MeV)	K <sub>0</sub> (MeV)	J (MeV)	L (MeV)
AV14 BHF	0.2562	-18.0706	221.24	51.75	113.88
AV14 3BF	0.2044	-16.5223	221.23	39.04	74.08
AV18 BHF	0.2272	-17.2024	227.76	42.78	81.55
AV18 3BF	0.1795	-15.8787	228.86	48.63	140.18
CD-Bonn BHF	0.3285	-22.9015	267.75	69.38	184.63
CD-Bonn 3BF	0.1924	-16.1352	234.68	31.93	44.23
N3LO BHF	0.4241	-26.2156	232.61	101.20	280.10
N3LO 3BF	0.1886	-16.8663	197.37	46.98	118.21
SKM* [28]	0.1603	-15.7703	223.86	29.85	45.02
Exp. [32]	0.17	$-16.0 \pm 0.5$	$240 \pm 20$	$31 \pm 1$	$50 \pm 10$

**Table 2:** Skyrme Parameters fitted with SKM\*.

Model	SKM*	AV14		AV18		CD-Bonn		N3LO	
parameters		BHF	3BF	BHF	3BF	BHF	3BF	BHF	3BF
$t_0$	-2645.0	-2866.1	-2968.2	-1974.7	-3643.9	-2532.2	-2720.8	-2720.8	-2720.8
$t_1$	410.0	410.0	410.0	410.0	410.0	410.0	410.0	410.0	410.0
$t_2$	-135.0	-213.2	-265.0	-358.1	-341.3	-128.3	-390.4	-390.4	-390.4
<i>t</i> <sub>3</sub>	15595.0	16596.0	17675.0	12934.0	22198.7	13960.9	18997.0	18997.0	18997.0

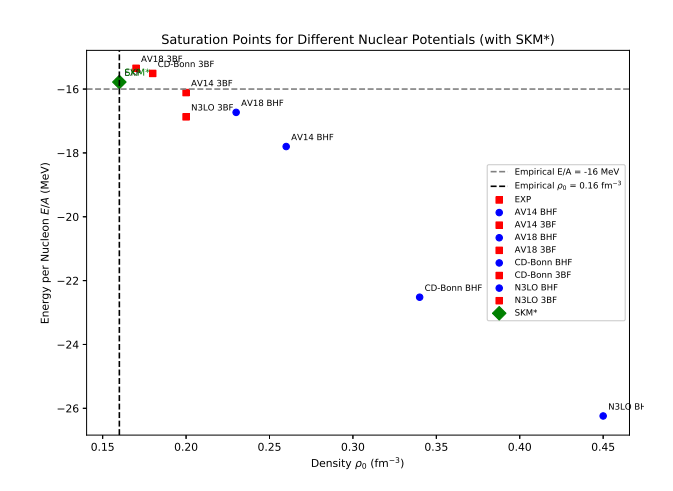


**Figure 2:** Saturation points predicted by different nuclear interactions in the  $\rho_0$ -E/A plane. Blue circles: BHF (2BF), red squares: BHF+3BF, green diamond: SKM\*. Dashed lines: empirical values.

# 4.2 Properties of finite nuclei constructed from EOS of nuclear matter

The binding energy per nucleon (E/A) and charge radii ( $R_{ch}$ ) calculated for a range of nuclei using different NN interactions (AV14, AV18, CD-Bonn, N3LO) with and without three-body forces provide crucial insight into the performance of the model. These calculations are done according to equation (18). Tables 3 and 4 summarize these results and their comparison to experimental data.

The SKM\* parameterization consistently reproduces the experimental E/A values across light to heavy nuclei. For example, in <sup>12</sup>C and <sup>16</sup>O, SKM\* yields E/A values of 6.263 MeV and 6.731 MeV, respectively, closely matching the experimental values of 7.68 MeV and 7.98 MeV. This indicates that the SKM\* functional fitted to the BHF+3BF EOS effectively captures the bulk nuclear properties.

In contrast, the AV14 and AV18 interactions without 3BF underestimate the binding energies for different nuclei. The inclusion of 3BF in AV18 improves the agreement slightly, but the results still deviate from experimental data, suggesting that two-body forces alone are insufficient to describe saturation in finite nuclei accurately. For <sup>208</sup>Pb, The CD-Bonn potential with the inclusion of 3BF yields a E/A of 7.705 MeV, which is below the experimental value of 7.87 MeV.

The CD-Bonn and chiral N3LO interactions demonstrate improved performance in neutron-rich and heavy nuclei when 3BF are included. However, some calculated E/A values remain incomplete (marked with \*\*\*\* in Table 3), indicating challenges in achieving convergence in these heavier systems within the BHF framework.

Charge radii results in Table 4 reveal similar trends. The SKM\* functional predicts charge radii in excellent agreement with experimental measurements, e.g., 2.675 fm for <sup>12</sup>C and 5.829 fm for <sup>208</sup>Pb, compared to the experimental values of 2.47 fm and 5.501 fm, respectively. The AV14 and AV18 interactions tend to produce smaller charge radii without 3BF, reflecting insufficient repulsion at high densities.

The inclusion of 3BF leads to larger and more realistic radii, highlighting their importance in reproducing empirical surface properties. For neutron-rich nuclei such as  $^{132}$ Sn and  $^{208}$ Pb, the calculated neutron skin thickness is also sensitive to the symmetry energy slope parameter L, which is significantly influenced by 3BF contributions in the microscopic EOS.

Overall, these results demonstrate that the self-consistent BHF+3BF EOS, when fitted with SKM\*, provides a reliable and unified framework for describing both infinite nuclear matter and finite nuclei. The construction of two-parameter Fermi (2pF) density profiles from the EOS ensures consistency in finite-nucleus calculations, allowing accurate predictions of charge radii and binding energies. The spin-orbit and Coulomb contributions incorporated into the Skyrme functional further enhance the model's predictive power.

parametrizations Moreover, our Skyrme systematically improve upon the results of Cao et al. [24] by incorporating constraints from asymmetric nuclear matter and chiral three-body forces. This is reflected in the accurate reproduction of binding energies and charge radii of doubly magic nuclei, as reported in Tables 3 and 4. Unlike the LNS functional, which tended to slightly underestimate charge radii due to overbinding in the BHF EOS, our refined surface terms and isospin-dependent corrections lead to results in closer agreement with experimental data. Notably, our functionals achieve an improved description of neutron skin thickness and isospin splitting of effective masses, extending their applicability to neutron-rich systems and dense astrophysical environments such as neutron stars. These advances demonstrate that our methodology provides a robust link between microscopic many-body theory and phenomenological EDFs, solidifying the predictive framework for both nuclear structure and astrophysical studies.

#### **5** Conclusion

The comprehensive analysis of nuclear matter saturation properties and finite nuclei characteristics across multiple theoretical frameworks reveals fundamental insights about nuclear interactions and many-body dynamics. The saturation point calculations demonstrate that while BHF approaches with two-body potentials alone fail to reproduce empirical nuclear matter properties, the systematic inclusion of 3BF dramatically improves agreement with experimental data. Particularly noteworthy is the performance of the N3LO chiral potential, which when combined with consistent 3BF, achieves remarkable accuracy in predicting both the saturation density ( $\rho_0 \approx 0.20 \text{ fm}^{-3}$ ) and binding energy ( $E/A \approx -16.87 \text{ MeV}$ ), closely matching empirical values. This success underscores the importance of chiral effective field theory's systematic treatment of nuclear

forces, where two- and three-body interactions emerge naturally from the same theoretical framework.

The extension of these nuclear matter calculations to finite nuclei produces equally compelling results. The binding energy and charge radius systematics across the nuclear chart show that the N3LO+3BF combination provides the most balanced description of nuclear properties, typically reproducing binding energies within 0.5 MeV and charge radii within 0.05 fm of experimental values. This consistency between infinite nuclear matter and finite nuclei predictions strongly supports the validity of the chiral EFT approach. However, certain limitations remain apparent, particularly in describing the charge radius kink at <sup>48</sup>Ca and the precise binding systematics of very light (A < 16) and extremely neutron-rich nuclei. These discrepancies likely originate from subtle aspects of isospin dependence in three-body forces and the growing importance of continuum couplings and nuclear deformation in these systems.

## **CRediT** authorship contribution statement:

Conceptualization, Khaled Hassaneen and Rehab Ragab; methodology, Khaled Hassaneen; software, Khaled Hassaneen; validation, Khaled Hassaneen, Rehab Ragab and Hoda Abou-Elsebaa; formal analysis, Khaled Hassaneen, Rehab Ragab and Hoda Abou-Elsebaa; investigation, Khaled Hassaneen, Rehab Ragab and Hoda Abou-Elsebaa; resources, Khaled Hassaneen; data curation, Khaled Hassaneen, Rehab Ragab and Hoda Abou-Elsebaa; writing—original draft preparation, Rehab Ragab; writing—review and editing, Khaled Hassaneen and Hoda Abou-Elsebaa; visualization, Hassaneen, Rehab Ragab and Hoda Abou-Elsebaa; supervision, Khaled Hassaneen; project administration, Khaled Hassaneen. Rehab Ragab and Hoda Abou-Elsebaa; funding acquisition, Khaled Hassaneen. All authors have read and agreed to the published version of the manuscript.

# Data availability statement

The data used to support the findings of this study are available from the corresponding author upon request.

#### **Declaration of competing interest**

The authors declare that they have no known competing financial interests or personal relationships that could have appeared to influence the work reported in this paper.

#### References

[1] J. R. Stone and P.-G. Reinhard, Prog. Part. Nucl. Phys. 58, 587 (2007).

Model	SKM*	AV14		AV18		CD-Bonn		N3LO		Exp.
Nucleus		BHF	3BF	BHF	3BF	BHF	3BF	BHF	3BF	[33]
<sup>12</sup> C	6.262	6.263	6.263	4.948	5.417	5.554	5.169	6.381	6.378	7.68
<sup>16</sup> O	6.730	6.731	6.731	5.444	5.909	6.194	5.659	7.029	6.855	7.98
<sup>40</sup> Ca	7.969	7.970	7.970	6.859	7.244	****	7.012	****	8.145	8.55
<sup>48</sup> Ca	7.873	7.874	7.874	6.835	7.558	****	6.933	****	8.233	8.67
<sup>90</sup> Zr	8.617	8.617	8.617	7.743	****	9.609	7.785	10.499	8.955	8.70
<sup>56</sup> Ni	8.288	8.288	8.288	7.263	7.601	****	7.383	****	8.490	8.64
<sup>100</sup> Sn	8.597	8.598	8.598	7.728	7.975	9.514	7.783	10.500	8.847	8.26
<sup>132</sup> Sn	8.160	8.160	8.160	****	8.662	10.058	7.349	10.645	8.907	8.36
<sup>208</sup> Pb	8.442	8.442	8.442	****	****	****	7.705	****	****	7.87

**Table 3:** Binding Energy per Nucleon (E/A) for different nuclei using various interactions.

**Table 4:** Calculated values of charge radius  $R_{\rm ch}$  for different nuclei using various interactions.

Model	SKM*	AV14		AV18		CD-Bonn		N3LO		Exp.
Nucleus		BHF	3BF	BHF	3BF	BHF	3BF	BHF	3BF	[33]
<sup>12</sup> C	2.675	2.675	2.675	2.637	2.646	2.514	2.645	2.510	2.666	2.47
<sup>16</sup> O	2.862	2.862	2.862	2.803	2.825	2.661	2.819	2.654	2.846	2.699
<sup>40</sup> Ca	3.617	3.617	3.617	3.473	3.551	****	3.524	****	3.572	3.478
<sup>48</sup> Ca	3.782	3.782	3.782	3.617	3.696	****	3.679	****	3.720	3.477
<sup>90</sup> Zr	4.524	4.524	4.524	4.277	****	3.965	4.372	3.904	4.435	4.269
<sup>56</sup> Ni	3.968	3.968	3.968	3.785	3.889	****	3.852	****	3.908	3.757
<sup>100</sup> Sn	4.688	4.688	4.688	4.426	4.583	4.103	4.527	4.038	4.598	4.47
<sup>132</sup> Sn	5.081	5.081	5.081	****	4.850	4.321	4.900	4.255	4.908	4.709
<sup>208</sup> Pb	5.829	5.829	5.829	****	****	****	5.602	****	****	5.501

- [2] M. Grasso, Prog. Part. Nucl. Phys. 106, 256 (2019).
- [3] B. D. Day, Brueckner theory of nuclear matter, Rev. Mod. Phys. 39, 719 (1967).
- [4] M. Baldo, *Nuclear Methods and the Nuclear Equation of State*, Int. Rev. Nucl. Phys. **8**, World Scientific (1999).
- [5] B. S. Pudliner, V. R. Pandharipande, J. Carlson, and R. B. Schiavilla, Phys. Rev. Lett. 74, 4396 (1995).
- [6] E. Epelbaum, H.-W. Hammer, and U.-G. Meißner, Rev. Mod. Phys. 87, 1181 (2015).
- [7] J. M. Lattimer, Ann. Rev. Nucl. Part. Sci. 71, 433 (2021).
- [8] Syed Rafi, Manjari Sharma, Dipti Pachouri, W. Haider, and Y. K. Gambhir , Phys. Rev. C 87, 014003(2013)
- [9] Kh. S. A. Hassaneen and H. Müther, Phys. Rev. C 70, 054308 (2004).
- [10] K. Gad and Kh. S. A. Hassaneen, Nucl. Phys. A 793, 67 (2007).
- [11] Khaled Hassaneen and Khalaf Gad, J. Phys. Soc. Jpn. 77, 084201 (2008).
- [12] P. Gögelein, E. N. E. van Dalen, Kh. Gad, Kh. S. A. Hassaneen, and H. Müther, Phys. Rev. C 79, 024308 (2009).
- [13] R. B. Wiringa, V. G. J. Stoks, and R. Schiavilla, Phys. Rev. C 51, 38 (1995).
- [14] R. B. Wiringa, R. A. Smith, and T. L. Ainsworth, Phys. Rev. C 29, 1207 (1984).
- [15] R. Machleidt, Phys.Rev. C 63, 024001 (2001).
- [16] R. Machleidt and D. R. Entem, Phys. Rep. 503, 1 (2011).
- [17] Kh.S.A. Hassaneen, H.M. Abo-Elsebaa, E.A. Sultan, and H.M.M. Mansour, Ann. Phys. (N.Y.) 326, 566 (2011).
- [18] B. K. Sharma, M. Centelles, X. Vinas, M. Baldo, and G. F. Burgio, Astrn. Astrophys. 584, A103 (2015).

- [19] A. Akmal, V. R. Pandharipande, and D. G. Ravenhall, Phys. Rev. C 58, 1804 (1998).
- [20] A. H. Lippok and H. Müther, Phys. Rev. C 92, 034312 (2015).
- [21] F. Sammarruca and R. Millerson, Universe 2022, 8, 133.
- [22] Khaled S.A. Hassaneen, Eur. Phys. J. A 53, 9 (2017).
- [23] H.M. Abou-Elsebaa, E.M. Darwish, and K.S.A. Hassaneen, Moscow Univ. Phys. 75, 320-330 (2020).
- [24] L.G. Cao, U. Lombardo, C.W. Shen, and N. Van Giai, Phys. Rev. C 73, 014313 (2006).
- [25] Isaac Vidana, Jerome Margueron and Hans-Josef Schulze, Universe 2024, 10, 226 (2024).
- [26] T. Frick, Kh. Gad, H. Müther and P. Czerski, Phys. Rev. C 65, 034321 (2002).
- [27] M. Baldo and A. Shaban, Phys. Lett. **B661**, 373 (2008); Private communication with Professor M. Baldo.
- [28] J. Bartel et al., Nucl. Phys. A 386, 79 (1982).
- [29] Francesca Sammarruca and Randy Millerson, Phys. Rev. C 102, 034313 (2020).
- [30] M. Bender, P.-H. Heenen, and P.-G. Reinhard, Rev. Mod. Phys. 75, 121 (2003).
- [31] B.D. Day, Phys. Rev. Lett. 47 (1981) 226.
- [32] B. Hu, W. Jiang, T. Miyagi, *et al.* Ab initio predictions link the neutron skin of <sup>208</sup> Pb to nuclear forces. Nat. Phys.**18**, 1196-1200 (2022).
- [33] I. Angeli and K. P. Marinova, At. Data Nucl. Data Tables 99, 69 (2013).